OPEN

Graphene from Amorphous Titanium Carbide by Chlorination under 200°C and Atmospheric Pressures

Tao Peng, Zongkui Kou, Hui Wu & Shichun Mu

State Key Laboratory of Advanced Technology for Materials Synthesis and Processing, Wuhan University of Technology, Wuhan 430070, PR China.

The synthesis of graphene via decomposition of SiC has opened a promising route for large-scale production of graphene. However, extremely high requirements for almost perfectly ordered crystal SiC and harsh process conditions such as high temperatures ($>1200°C$) and ultra-high vacuum are two significant challenges hindering its wide use to synthesize graphene by decomposition of SiC. Here, we show that the readily available precursor of carbides, amorphous TiC ($a-Ti_{1-x}C_x$), can be transformed into graphene nanosheets (GNS) with tunable layers by chlorination method at very low temperatures ($200°C$) and ambient pressures. Moreover, freestanding GNS can be achieved by stripping off GNS from the surface of resulting particles. Therefore, our strategy, the direct transformation of $a-Ti_{1-x}C_x$ into graphene, is simple and expected to be easily scaled up.

Graphene, the first two-dimensional atomic crystal available to us[1], has been the focus of infinite research since its discovery in 2004[2], because of its fascinating properties, such as the giant electron mobility, large specific surface area, high thermal and electric conductivities, and high chemical stability[2–5]. Such excellent properties make it glamorous for numerous potential applications. For example, the large specific surface area, and high thermal and electric conductivities make it attractive for use in energy-storage materials, catalysts, photo-catalysts, solar energy materials, chemical sensors, field-effect transistors and optoelectronic devices[4,5]. However, the large-scale production of graphene by a facile synthesis method becomes a bottleneck in developing graphene-based materials.

Various synthesis techniques have been developed and exploited to prepare graphene with various layers, dimensions, shapes and quality[1]. For example, micromechanical cleavage has been developed to produce graphene[2]. However, it is difficult to envisage how to scale up this process. Although exfoliation of graphite or graphite derivatives by solution-based process enables the synthesis of graphene-like sheets on a large scale[6,7], the number of graphene layers cannot be controlled and the graphene layers readily stack into multilayer (more than 10-layer) owing to the strong π-π interaction between graphene layers, which limits its further applications[8]. In comparison, few-layer graphene films have been produced via chemical vapor deposition on copper foils and films[9]. Although this method can produce high quality graphene, its large-scale production is limited due to high energy consumption[1].

Graphene with tunable layers has been grown by thermal decomposition of silicon carbide (SiC) wafers[10,11]. High quality graphene, with crystallites approaching even hundreds of micrometers in size, can be generated via the epitaxial growth method[12–14]. In particular, the monolayer or bilayer graphene on crystal SiC wafers has been exfoliated by means of the stress induced with a Ni film and transferred to another substrate[15]. However, this method is significantly prohibited by high quality substrate requirements, high synthesizing temperatures and expensive ultra-high vacuum (UHV) operation. In addition, the graphene formed on crystal SiC such as 6*H*-SiC has a very strong interaction with crystal SiC substrates[26], making it extremely difficult to peel off the graphene layers. Recently, the amorphous SiC ($a-Si_{1-x}C_x$) nano-film on granules has been directly transformed into GNS under the temperature of 800°C and ambient pressures in chlorine atmosphere[16]. It is potential to produce graphene at large scale by using very low cost amorphous carbide granules as well as the relatively facile process conditions such as relatively low temperatures and ambient pressures. Moreover, it is very promising to further lower the temperature of chlorination and to tune the layer of graphene effectively. However, temperatures below 650°C are not sufficient to remove Si from SiC[17]. According to previous reports, titanium carbide (TiC) shows higher reactivity than SiC, and the reaction temperature almost has no influence on the rate of etching TiC[17,18].
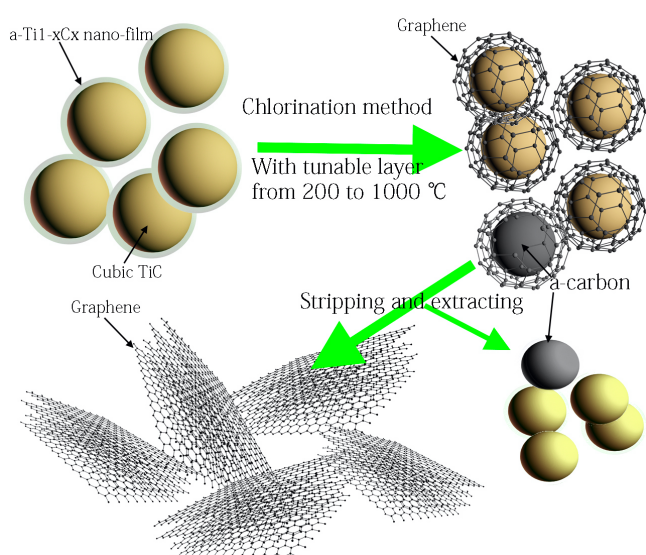
Figure 1 | Schematic of the transformation of the TiC NPs into GNS, and then GNS are stripped off from granules. TiC NPs with a layer of a-Ti$_{1-x}$C$_x$ nano-films are shown in the upper left; the upper right shows the integral GNS as shield covering the TiC core and carbon NPs; the lower left shows GNS; the lower right shows TiC and carbon NPs.

Therefore, it is expected to significantly lower the reaction temperature of chlorination by using amorphous titanium carbide (a-Ti$_x$C$_{1-x}$) granules as precursors. We note that a-Ti$_{1-x}$C$_x$ is a readily available material at a low cost. Different from the crystal SiC such as anisotropic 6H-SiC(0001), the transformation of a-Ti$_{1-x}$C$_x$ into graphene is not associated with the orientation of a-Ti$_{1-x}$C$_x$ surfaces

because of its amorphous and isotropic properties. In addition, according to the report, chlorination is a very economic and scalable method to produce carbide-derived carbon (CDC) materials[19], so the chlorination method is very promising to be widely used in producing graphene.

Here, we demonstrate that the amorphous TiC (a-Ti$_{1-x}$C$_x$) nano-film can be transformed into GNS by chlorination at very low temperatures (200°C) and ambient pressures, and the number of graphene layers was tuned by controlling chlorination temperatures. Furthermore, the effect of size of TiC particles on the number of graphene layers was also investigated and the resulting GNS from titanium carbide-derived carbon nanoparticles (NPs) chlorinated at 200°C (TiC-CDC-200) were stripped off and extracted (Fig. 1). This novel synthetic approach is simple and potential for large volume production of graphene. This study was conducted on TiC nano-powders with core-shell structures where the cubic TiC nanocrystal was a core, and the amorphous Ti$_{1-x}$C$_x$ (a-Ti$_{1-x}$C$_x$) nano-film was a shell (Fig. S1). The typical high resolution transmission electron microscopy (HRTEM) images of as-received nano-TiC and the resulting titanium carbide-derived carbon chlorinated at 200°C (TiC-CDC-200) are shown in Fig. 2 a–e. It can be seen that TiC NPs are uniform, and their average particle size is approximately 40 nm (Fig. 2a). All TiC NPs with cubic TiC (Fig. S2) cores are surrounded by a-Ti$_{1-x}$C$_x$ nano-films with thickness of about 5 nm (Fig. 2b). After chlorination under ambient pressures at 200°C, the resulting TiC-CDC-200 NPs kept almost the same in shape and volume as those of TiC precursors, which is consistent with the conformal transformation[20]. Notwithstanding the almost constant shape and volume, the surface of TiC-CDC-200 NPs underwent significant modifications compared with TiC NPs. Also, the current density and specific capacitance of TiC-CDC-200 significantly exceeds those of reduced graphene oxide (RGO) (Fig. S3), indicating the good electro-conductivity and high specific surface area of TiC-
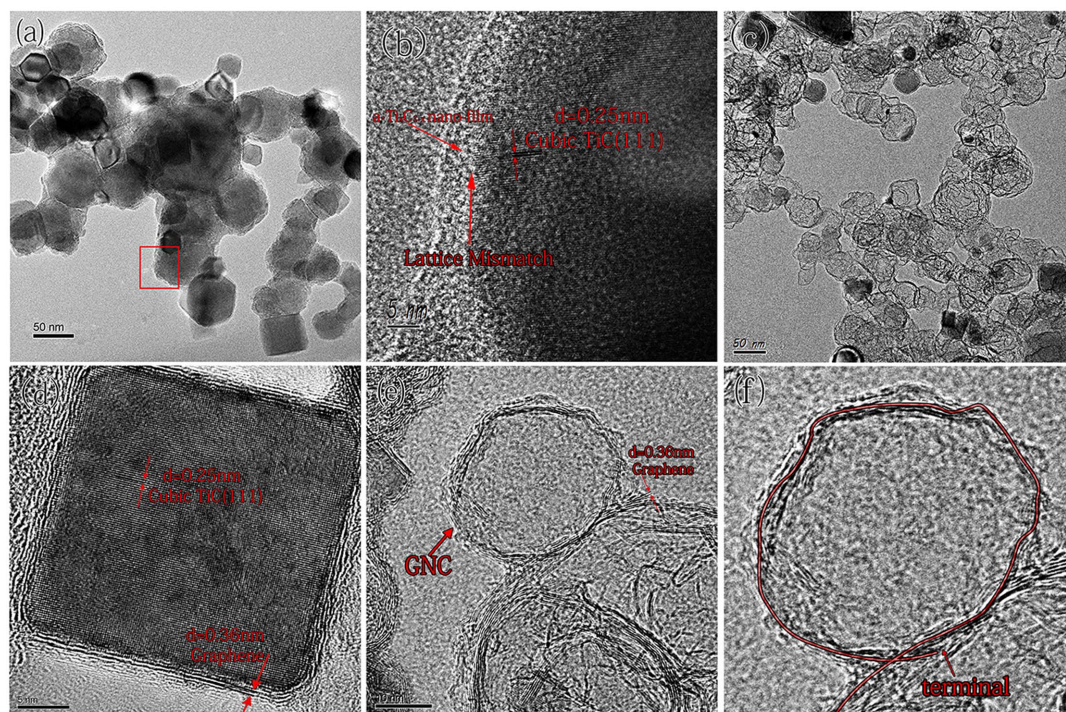
Figure 2 | (a) TiC NPs HRTEM images. **(b)** The magnified image of the rectangle area in (a), showing the a-Ti$_{1-x}$C$_x$ nano-film are clearly evident and the lattice mismatch between a-Ti$_{1-x}$C$_x$ nano-films and cubic TiC substrates. **(c)** The HRTEM image of TiC-CDC-200 NPs after chlorination, showing all NPs are covered by GNS. **(d)** The HRTEM image of TiC-CDC-200 NPs after TiC chlorination, showing integral GNS as a layer covering TiC NPs and as shields protecting the cubic TiC core from Cl$_2$ etching. **(e)** The HRTEM image of graphene nano-curl (GNC) and TiC-CDC-200 NPs after TiC chlorination, showing porous GNS covers the amorphous carbon, which could not protect the core like the integral GNS did. **(f)** The magnification of GNC in (e), showing the exfoliated GNS were curled on the surface of particles.
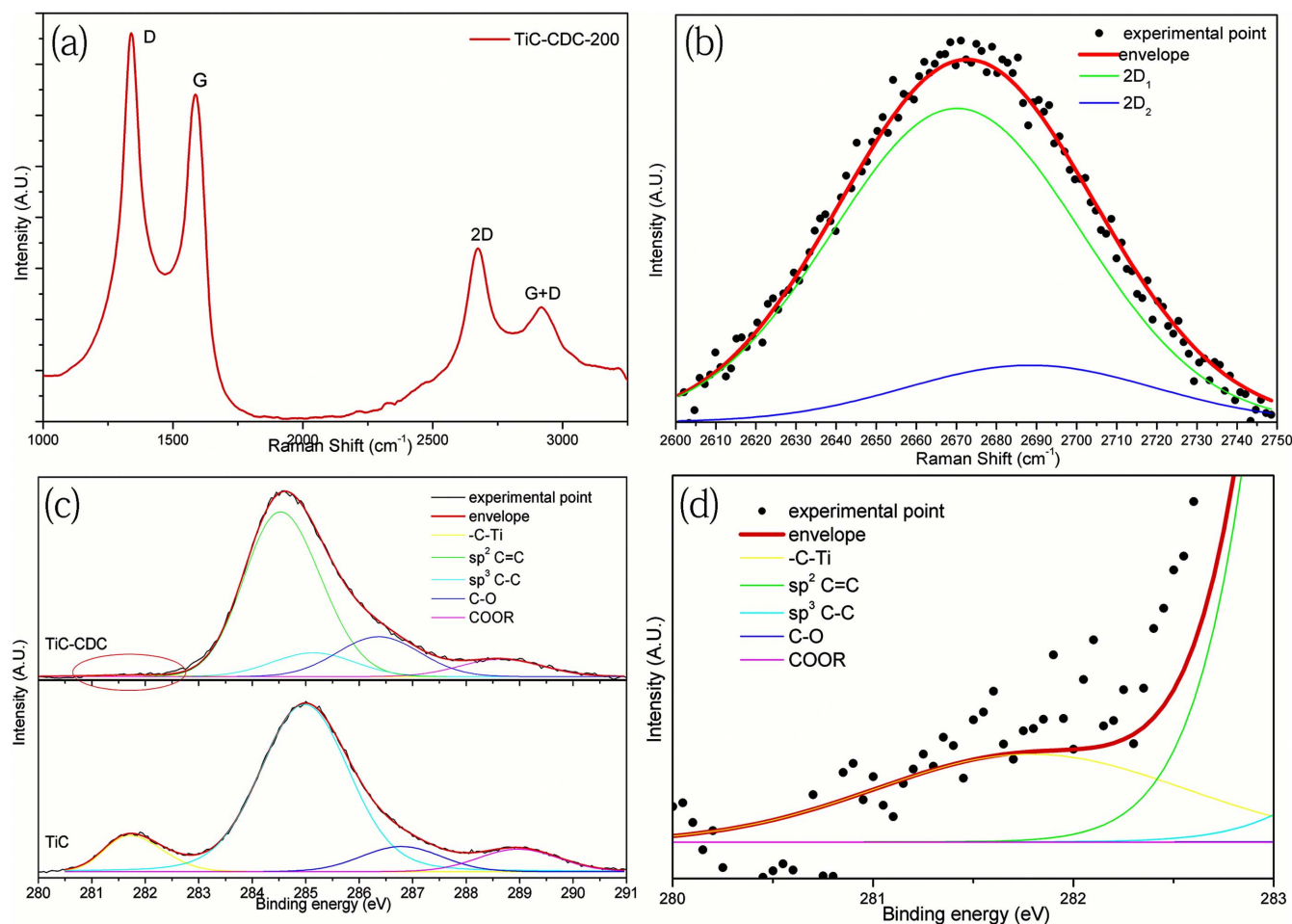
Figure 3 | (a) Raman-scattering spectra from TiC-CDC-200 NPs. (b) Magnification of the 2D line in (a) showing the two inner peak $2D_1$ (2670.6 cm^{-1}) and $2D_2$ (2689.0 cm^{-1}) of the 2D band in multi-layer graphene. (c) C1s XPS spectra of TiC-CDC-200 and TiC NPs. The TiC-CDC carbon peak can be fitted using five components including both sp^2 and sp^3 bonded carbon, while the TiC carbon peak is without sp^2 C=C components. (d) The magnification of the -C-Ti peak of TiC-CDC in red circle of (c), indicating the residual TiC after chlorination.

CDC-200 NPs. All TiC-CDC-200 NPs were covered with finely few-layer graphene formed by chlorinating the a-Ti$_{1-x}$C$_x$ nano-film (Fig. 2 c–f). These changes on surfaces indicate that the a-Ti$_{1-x}$C$_x$ nano-film was transformed into graphene.

It can be found that the cores covered with few-layer graphene are usually of two types, namely a cubic TiC core (Fig. 2d) or an amorphous core (Fig. 2e). It is well known that graphene is almost completely impermeable to any gases[1], hence, once the continuous GNS were formed as the covering layer wrapping up TiC NPs, it would prevent TiC from being further etched using Cl$_2$ due to a shield effect of graphene, which left behind the cubic TiC core, in good agreement with the results of XRD and selected area electron diffraction (SAED) patterns of the TiC-CDC product (Fig. S2 and Fig. S4). By contrast, if defects or pores existed in GNS, the porous GNS could not act as a shield to protect the inner core from being etched in Cl$_2$, thus leaving behind the amorphous carbon (a-C) core (Fig. 2e). Especially, a graphene nano-curl (GNC) architecture on the surface is present in Fig. 2e where few-layer graphene is curled and partly exfoliated. Further magnification of Fig. 2e shows the terminal of GNC (Fig. 2f). These indicate that it is relatively easy to peel off the resulting GNS in comparison with graphitic shells or carbon onions[21], owing to the weak cohesive strength of the graphene/TiC interface. Therefore, after Ti atoms were etched away with Cl$_2$, the a-Ti$_{1-x}$C$_x$ nano-film can be converted into GNS with GNC architectures based on two types of cores (cubic TiC or amorphous carbon cores) (Fig. 1), which mainly depend upon the continuity and integrity of GNS.

The presence of GNS was also demonstrated by both Raman spectroscopy and X-ray photoelectron spectroscopy (XPS) techniques as shown in Fig. 3. Raman spectrum of TiC-CDC-200 (Fig. 3a) has high intensity of D (1320 cm^{-1}) and G (1591 cm^{-1}) bands, which is attributed to a large amount of amorphous carbon in the form of cores and defects in GNS. Significantly, the presence of 2D and D+G peak hints very positive information, as compared with Raman spectrum of TiC NPs (Fig. S5). The low intensities of the 2D peak and I_{2D}/I_G are owing to the relatively low content ratio of graphene to amorphous carbon in TiC-CDC NPs. However, compared with the 2D peak of graphite[22], the 2D peak of TiC-CDC has downshifted, indicating a high intensity ratio of $2D_1$ (2670 cm^{-1}) component to $2D_2$ (2690 cm^{-1}) component (Fig. 3b). It is well known that the 2D peak in bulk graphites and multi-layer graphene consists of $2D_1$ and $2D_2$ components, and further decrease in layer numbers of graphene leads to a significant increase in the intensity of $2D_1$ component[22–25]. In particular, the monolayer graphene has a much narrower and down-shifting 2D peak as compared with the multi-layer graphene[23,24]. Therefore, based on the Raman data, the very high percentage of $2D_1$ component to $2D_2$ component indicates that the number of graphene layers is mainly two although a small parts of monolayer and few (from three to five) layers can be found in TiC-CDC-200 samples, which is in good agreement with the HRTEM results (Fig. 3 c–d).

Shown in Fig. 3 c and d are the XPS spectra of TiC-CDC-200 and TiC NPs. TiC NPs have four components with binding energies of

281.7, 285.0, 286.6 and 288.9 eV, which correspond to -C-Ti bonding, sp^3 bonded carbon, -C-O and -COOR bonding, respectively. The presence of sp^3 C-C bonds in samples is attributed to the disordered a-$Ti_{1-x}C_x$ structure, which is in consistence with the results from the Raman analyses of TiC (Fig. S5). Meanwhile, the carbon peak of the TiC-CDC-200 not only has four components, but shows an extra component of sp^2 bonded carbon at 284.5 eV, mainly owing to the coexistence of graphene and amorphous carbon. Additionally, it also shows sharply decreased intensities of –C-Ti and sp^3 C-C (Fig. S6), revealing the successful transformation of TiC into carbon materials including amorphous carbon and graphene. Such low intensity of –C-Ti is another important evidence of the presence of TiC cores, which is consistent with the results from HRTEM (Fig. 2c).

Significantly, it is interesting to note that the number of graphene layers can be tuned by controlling temperatures. Shown in Fig. 4a is the Raman spectrum of TiC-CDC under reaction temperatures from 200 to 1000°C. They all show high intensity of D (1320 cm^{-1}) to G (1591 cm^{-1}) bands, mainly owing to the very high content of amorphous carbon cores. What's more, the 2D peak is gradually up-shifting from 2673 (200°C) to 2686 cm^{-1} (1000°C) and the intensity of the 2D peak decreases with temperatures. For these 2D peaks, the percentage of $2D_1$ (2670 cm^{-1}) component decreases with temperatures, while the percentage of $2D_2$ (2691 cm^{-1}) component increases correspondingly (Fig. 4b), which indicates the increase in the number of graphene layers. The number of graphene layers was mainly monolayer and bilayer in TiC-CDC-200. With temperature rising, the few-layer (more than three layers but less than 10 layers) graphene became dominant. Especially, the percentage of $2D_2$ of TiC-CDC-1000 exceeds that of $2D_1$, indicating most graphene was more than five layers which is in very good agreement with TEM results.

HRTEM images of TiC-CDC-600 and TiC-CDC-1000 are shown in Fig. 4c and d, respectively. The number of graphene layers is usually about five in TiC-CDC-600 and about eight in TiC-CDC-1000, which is greater than that of TiC-CDC-200 (Fig. 2c and d). As reported, the formation of graphene is the result of the collapse of the highly defective carbon layers[11] that are formed via subtracting Ti from a-$Ti_{1-x}C_x$ by Cl_2. Therefore, the increase in layer numbers of graphene can be attributed to the increased Ti etching rate at elevated temperatures that gives rise to thicker defective C-rich layers and subsequently collapses into more layers of graphene[16]. Besides the synthesizing temperatures, the size of TiC particles also affects the number of graphene layers. Compared with chlorination of TiC NPs, the chlorination of TiC micro-particles (around 1 μm) only occurred at higher temperatures (no less than 400°C), and the number of graphene layers in TiC-CDC micro-particles (micro-TiC-CDC) exceeded that of TiC-CDC NPs produced at the same temperature (Fig. S8 and S9). The number of graphene layer was around five in micro-TiC-CDC-400 (Fig. S8b) and around eight in micro-TiC-CDC-600 (Fig. S8c). With temperature rising, the number of graphite layers was more than ten in both micro-TiC-CDC-800 and micro-TiC-CDC-1000 samples, which is in good agreement with HRTEM results (Fig. S8d).

In order to achieve freestanding GNS, we separated GNS from the surface of TiC-CDC NPs. After separated from TiC-CDC-200 NPs, the resulting freestanding GNS are shown in the Fig. 4e. And the remnant amorphous carbon and TiC cores without the coverage of GNS are also exhibited in Fig. S7. As mentioned earlier, the presence of GNC architectures (Fig. 2e) can promote the exfoliation of GNS from CDC NPs. Differently from the single crystal of 6H-SiC[11,26], the significant difference between disordered a-$Ti_{1-x}C_x$ and ordered cubic TiC substrates (Fig. 2b) contribute directly to interface mismatch, leading to the weak interaction between disordered a-$Ti_{1-x}C_x$-derived GNS and cubic TiC substrates. As shown in Fig. 4f, the freestanding GNS obviously shows a lower I_D/I_G (0.52) and higher I_{2D}/I_G (0.58) than I_D/I_G (1.26) and I_{2D}/I_G (0.51) of TiC-CDC-200 (Fig. 3a). The decrease of I_D/I_G suggests the presence of larger crys-

talline size or a higher graphitization degree in GNS[29,30], indicating a relative good quality for freestanding GNS.

What is the reason for the formation of GNS via chlorination of a-$Ti_{1-x}C_x$ nano-films? One of key factors for achieving graphene is the formation of noncarbon-atom vacancies in carbide substrates[11]. For vacuum decomposition of SiC, the Si vacancy is created when Si atoms of topmost SiC bi-layer leave their position and C atoms of the top SiC bi-layer[26]. Eventually, these highly defective C-rich layers is condensed into a thermally stable graphene[11,26]. Similarly, such processes also happen when carbides are etched with chlorination. Therefore, the occurrence of GNS is owing to the condensation of the highly defective C-rich layers created by Ti vacancies by extracting Ti atoms in the a-$Ti_{1-x}C_x$ nano-film by means of Cl_2 etching.

Meanwhile, there are at least three possible reasons for understanding the much milder conditions in comparison with the extremely harsh conditions used in the SiC crystal annealing process. The first is the long-range disordered lattice of a-$Ti_{1-x}C_x$ nano-film (Fig. S1). Compared with the graphitization of crystal SiC, the graphitization of a-$Ti_{1-x}C_x$ can skip a redundant step (very high energy barrier) in which the long-range ordered phase is converted into the long-range disordered intermediate phase in graphene formation. The second possibility is the enhanced extraction of Ti atom from lattice by Cl_2 etching. As compared with very slow extraction of Si or metal atoms in carbides under high-temperature or UHV conditions[11,28], the extraction of Si or metal atoms from lattices can be significantly enhanced by Cl_2 etching[19,27,28]. Therefore, the very high synthesis temperatures and the UHV requirements can be remarkably removed by chlorination. The third is probably due to the more reactivity of TiC than that of SiC. The etching of a-$Si_{1-x}C_x$ with Cl_2 also gives rise to formation of graphene at the relative high temperature of 800°C compared with 200°C for a-$Ti_{1-x}C_x$ nano-films, because SiC shows lower reactivity than TiC[17], which leads to a reduced Si extraction. Hence, the relatively high reactivity of TiC can largely reduce the synthesis temperatures and the UHV requirements.

In summary, we have shown the growth of GNS from a-$Ti_{1-x}C_x$ nano-films by chlorination at temperatures as low as 200°C under ambient pressures. The number of graphene layers was able to increase by elevating a chlorination temperature and utilizing larger size TiC particles. No requirements for highly oriented crystal carbide such as 6H-SiC (0001) and high temperature annealing in ultra-high vacuum make this approach very facile. Moreover, the chlorination is now a very economic and scalable method. Further research is desirable for a thorough understanding of the mechanism and influence of the process parameters on the graphene formation from a-$Ti_{1-x}C_x$. Especially, the number of graphene layers might be also finely tuned by controlling other key factors such as the thickness and the x value of a-$Ti_{1-x}C_x$ nano-films.

Methods

The TiC nano-powders and TiC micro-powders with a-$Ti_{1-x}C_x$ nano-film were bought from Kaier Nano Co. and used as-received. The TiC nano-powders were placed into a horizontal hot-wall tubular flow reactor operated at ambient pressures. The reactor was first filled with pure He gas to remove air. Then the reactor was heated to reaction temperature under pure He and the samples were exposed to a He/Cl_2 gas mixture for 40 min. After filled with pure He gas for 30 min to remove residual Cl_2 and $TiCl_4$, the furnace was heated or cooled to 600°C to further remove Cl_2 and $TiCl_4$. Finally, the furnace was cooled down to room temperature under pure He. All the exhaust gases of this experiment were neutralized at the reactor exit by bubbling through a 30% NaOH solution. In our experiment, titanium carbide-derived carbon (TiC-CDC) was produced at temperatures from 200 to 1000°C. For comparison purposes, TiC micro-powders followed a similar procedure. The TiC nano- and micro-powders were transformed into the TiC-CDC by selective etching of Ti atoms in chlorine atmosphere under reaction temperatures from 200°C to 1000°C and ambient pressure via:

$$Ti_{1-x}C_x(s) + 2(1-x)\ Cl_2(g) \rightarrow (1-x)\ TiCl_4(g) + xC(s) \tag{1}$$
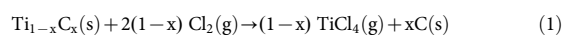
For producing freestanding GNS, 1 g of TiC-CDC-200 nano-powder, 50 mL of Sulfuric acid (98%) and 1 g of sodium nitrate were mixed in a three necked flask
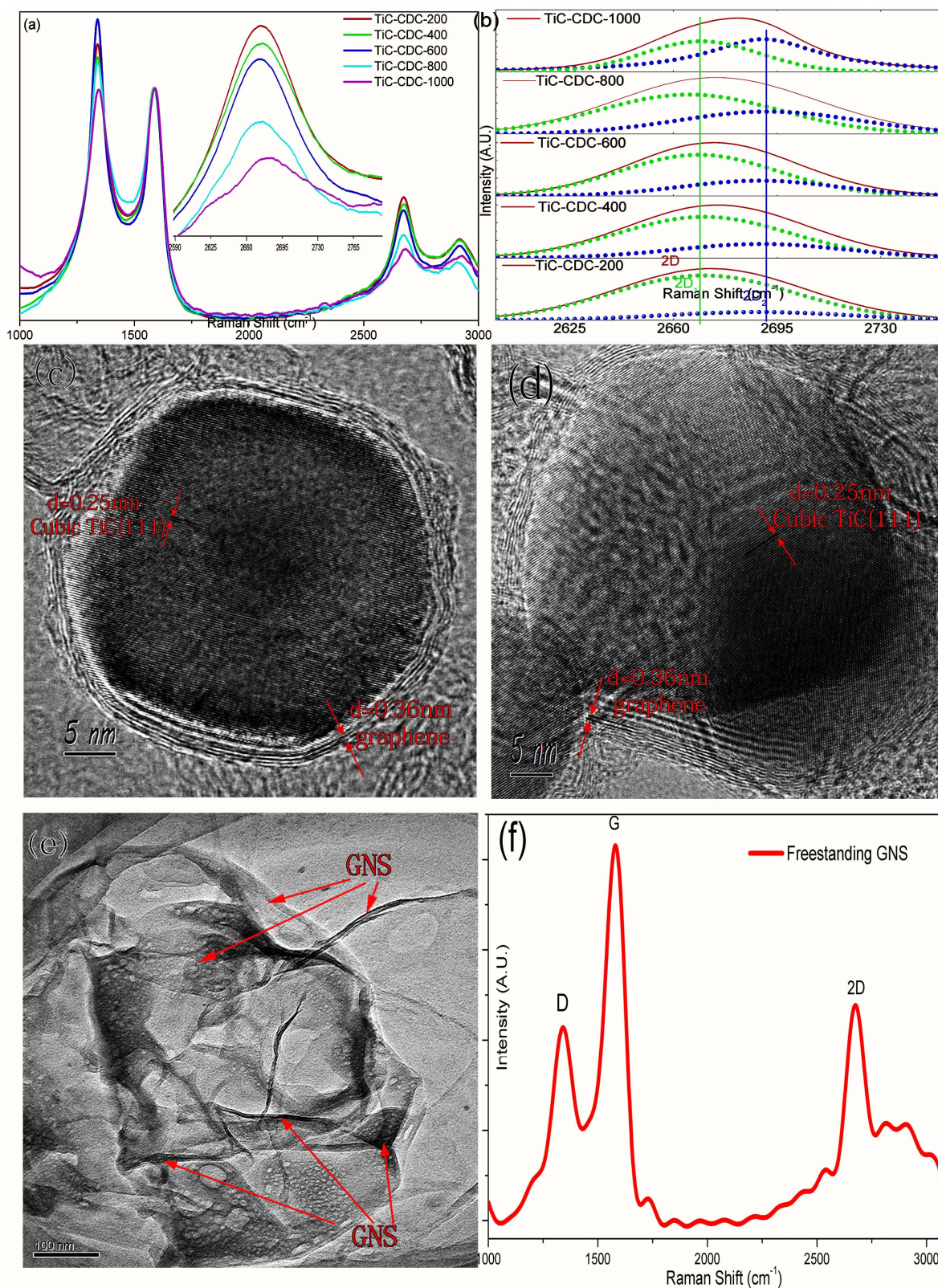
Figure 4 | (a) Raman spectra of TiC-CDC synthesized at different temperatures. It has been normalized by the intensity of G-peak. The magnified image in the inset shows the up-shifting of 2D peaks from 2673.3 cm^{-1} (200°C), to 2674.4 cm^{-1} (400°C), to 2679.1 cm^{-1} (600°C), to 2680.7 cm^{-1} (800°C), and to 2686.5 cm^{-1} (1000°C). (b) Magnification of the 2D peaks in (a). The peak fit of the 2D$_1$ (2670 cm^{-1}) and 2D$_2$ (2691 cm^{-1}) components to the 2D TiC-CDC band is shown. All peaks are amplitude normalized and vertically offset. (c) The HRTEM image of TiC-CDC NPs after TiC chlorination at the higher temperature of 600°C, showing about 5 layers graphene as covering layer wrapping up TiC NP (d). The HRTEM image of TiC-CDC NPs after TiC chlorination at higher temperature 1000°C, showing about 8 layers graphene with break as covering layer wrapping up the amorphous carbon. (e) The freestanding GNS separated from TiC-CDC-200. (f) Raman spectra of freestanding graphene generated by peeling TiC-CDC-200 NPs.

(500 mL), and were vigorously stirred at room temperature. After a period of time, in the process of stirring, 6 g of potassium permanganate was added into the three necked flask. The color of mixture became black-and-green, then the mixture was heated up to 40°C. After stirred for 12 h under temperature of 40°C, the mixture became dry and grey. Again, 100 mL Sulfuric acid (98%) and 3 g of potassium permanganate were added into the three necked flask, which gave rise to a green mixture. The mixture was stirred continuously for 12 h without a stop. After the color became shallow celadon, the mixture was cooled to room temperature. In the process of mechanical agitation, 300 mL water was added, and the color turned light-red. Finally, 10 mL of hydrogen peroxide (30 wt%) was added to the mixture, which gave rise to a supernatant and a golden-yellow precipitate at the bottom of the flask. This supernatant contained GNS was subsequently deposited on a carbon film and dried at room temperature for HRTEM tests.

An argon ion laser operated at a wavelength of 514.5 nm was utilized as the excitation light source for Raman analysis. In order to achieve more accurate Raman results, we did Raman test from 100 to 3300 cm^{-1} and set the accumulation times as 20 for high S/N ratio. The microstructures of the as-received TiC nano-powders and the as-prepared TiC-CDC were characterized using JEOL 2010 high resolution transmission electron microscopy (HRTEM). All samples were dispersed ultrasonically in ethanol. An aliquot of this solution was deposited on a carbon film and dried at room temperatures before characterization. XPS measurements were performed with a VG Scientific ESCALAB 210 electron spectrometer using Mg Kα radiation (hm=1253.6 eV, 300 W) under a vacuum of 2×10^{-8} Pa. The binding energy was referenced to the C 1 s line at 284.5 eV. The error in the determination of electron binding energies and line widths did not exceed 0.2 eV. The X-ray diffraction (XRD) analysis was performed using a Rigaku X-ray diffractometer equipped with CuKá radiation source. The XRD patterns were collected using step scans with a step of 0.01° 2 θ and a count time of 2 s per step between 10° and 80° 2θ.

For preparing working electrodes, 3 mg of TiC-CDC-200 powder was dispersed in 1000 uL of deionized water and then mixed with 100 uL 5 wt% perfluorosulfonic acid (PSFA) Nafion (DuPont Co.) solution in an ultrasonic ethanol bath for 30 min to form well-dispersed ink, and then 10 uL of such ink was coated on a mirror-polished glassy carbon disk electrode (5 mm in diameter) as working electrode, respectively. The electrochemical performance of samples was conducted by a computer controlled Autolab PGSTAT 30 potentiostat (Eco Chemie B.V, Holland) with a three-electrode cell setup. A platinum electrode was used as the counter electrode, while a Hg/Hg$_2$Cl$_2$ electrode was employed as the reference electrode. All potentials measured were referred to the normal hydrogen electrode (NHE). Electrolyte solutions (0.5 M H$_2$SO$_4$ solution at 25°C) were deaerated by high purity nitrogen for 30 min prior to any electrochemical measurements. For comparison purposes, RGO and Vulcan XC-72 followed a similar procedure.

1. Novoselov, K. S. *et al*. A roadmap for graphene. *Nature* **490**, 192–200 (2012).
2. Novoselov, K. S. *et al*. Electric field effect in atomically thin carbon films. *Science* **306**, 666–669 (2004).
3. Novoselov, K. S. *et al*. Two-dimensional gas of massless Dirac fermions in graphene. *Nature* **438**, 197–200 (2005).
4. Geim, A. K. & Novoselov, K. S. The rise of graphene. *Nat. Mater.* **6**, 183–191 (2007).
5. Yin, Z. *et al*. Graphene-Based Materials for Solar Cell Applications. *Adv. Energy Mater.* **4**, 1300574–130072 (2014).
6. Hernandez, Y. *et al*. High-yield Production of graphene by liquid-phase exfoliation. *Nature Nanotech.* **3**, 563–568 (2008).
7. Stankovich, S. *et al*. Graphene-based composite materials. *Nature* **442**, 282–286 (2006).
8. Lotya, M. *et al*. Liquid Phase Production of Graphene by Exfoliation of Graphite in Surfactant/Water Solutions. *J. Am. Chem. Soc.* **131**, 3611 (2009).
9. Li, X. *et al*. Large-Area Synthesis of High-Quality and Uniform Graphene Films on Copper Foils. *Science* **324**, 1312–1314 (2009).
10. Bolen, M. L., Harrison, S. E., Biedermann, L. B. & Capano, M. A. Graphene formation mechanisms on 4H-SiC(0001). *Phys. Rev. B* **80**, 115433 (2009).
11. Forbeaux, I., Themlin, J. M. & Debever, J. M. Heteroepitaxial graphite on 6H-SiC (0001): Interface formation through conduction-band electronic structure. *Phys. Rev. B* **58**, 16396–16406 (1998).
12. Virojanadara, C. *et al*. Homogeneous large-area graphene layer growth on 6H-SiC(0001). *Phys. Rev. B* **78**, 245403 (2008).
13. Kim, S., Ihm, J., Ihm, J., Choi, H. J. & Son, Y. W. Origins of anomalous electronic structures of epitaxial graphene on silicon carbide. *Phys. Rev. Lett.* **100**, 176802 (2008).
14. Deng, D. *et al*. Freestanding Graphene by Thermal Splitting of Silicon Carbide Granules. *Adv. Mater.* **22**, 2168–2171 (2010).
15. Kim, J. *et al*. Layer-Resolved Graphene Transfer via Engineered Strain Layer. *Science* **342**, 833–836 (2013).
16. Peng, T., Lv, H. F., He, D. P., Pan, M. & Mu, S. C. Direct Transformation of Amorphous Silicon Carbide into Graphene under Low Temperature and Ambient Pressure. *Sci. Rep.* **3**, 1148 (2013).
17. Popovska, N. & Kormann, M. Processing of porous carbon with tunable pore structure by the carbide-derived carbon method. *JOM.* **62**, 6 (2010).
18. Kormann, M., Ghanem, H., Gerhard, H. & Popovska, N. Processing of carbide-derived carbon (CDC) using biomorphic porous titanium carbide ceramics. *J Eur Ceram Soc.* **28**(6), 1297–303 (2007).
19. Presser, V., Heon, M. & Gogotsi, Y. Carbide-Derived Carbons – From Porous Networks to Nanotubes and Graphene. *Adv. Funct. Mater.* **21**, 810–833 (2011).
20. Gogotsi, Y. *et al*. Nanoporous carbide-derived carbon with tunable pore size. *Nature Mater.* **2**, 591–594 (2003).
21. Banhart, F. & Ajayan, P. M. Carbon onions as nanoscopic pressure cells for diamond formation. *Nature* **382**, 433–435 (1996).
22. Nemanich, R. J. & Solin, S. A. First- and second-order Raman scattering from finite-size crystals of graphite. *Phys. Rev. B* **20**, 392–401 (1979).
23. Ferrari, A. C. *et al*. Raman Spectrum of Graphene and Graphene Layers. *Phys. Rev. Lett.* **97**, 187401 (2006).
24. Chen, Z. P. *et al*. Three-dimensional flexible and conductive interconnected graphene networks grown by chemical vapour deposition. *Nature Mater.* **10**, 424–428 (2011).
25. Chae, S. J. *et al*. Synthesis of Large-Area Graphene Layers on Poly-Nickel Substrate by Chemical Vapor Deposition: Wrinkle Formation. *Adv. Mater.* **21**, 2328 (2009).
26. Emtsev, K. V. *et al*. Interaction, growth, and ordering of epitaxial graphene on SiC{0001} surfaces:A comparative photoelectron spectroscopy study. *Phys. Rev. B* **77**, 155303 (2008).
27. Pérez, C. R. *et al*. Structure and Electrochemical Performance Carbide-Derived Carbon Nanopowders. *Adv. Funct. Mater.* **23**, 1081–1089 (2013).
28. Gogotsi, Y., Welz, S., Ersoy, D. A. & McNallan, M. J. Conversion of silicon carbide to crystalline diamond-structured carbon at ambient pressure. *Nature* **411**, 283–287 (2001).
29. Ferrari, A. C. & Robertson, J. Interpretation of Raman spectra of disordered and amorphous carbon. *Phys. Rev. B* **61**, 14095–14107 (2000).
30. Tuinstra, F. & Koenig, J. L. Raman Spectrum of Graphite. *J. Chem. Phys.* **53**, 1126–1130 (1970).

Acknowledgments

Author contributions

S.M. proposed and supervised the project, T.P. and S.M. designed the experiments, T.P. performed experiments under the help of Z.K., H.W. T.P. and S.M. analysed data and wrote the manuscript. All the authors participated in discussions of the research.

Additional information